

# Axisymmetric Vortices in Spinor Bose-Einstein Condensates under Rotation

Tomoya Isoshima<sup>1,\*</sup> and Kazushige Machida<sup>2</sup>

<sup>1</sup> *Materials Physics Laboratory, Helsinki University of Technology,  
P. O. Box 2200 (Technical Physics), FIN-02015 HUT, Finland*

<sup>2</sup> *Department of Physics, Okayama University, Okayama 700-8530, Japan*  
(Dated: October 30, 2018)

The relative stability of various axisymmetric vortices in a spinor Bose-Einstein condensate with  $F = 1$  is examined within extended Bogoliubov theory. This yields the phase diagram in the plane of external rotation frequency vs magnetization. We compare antiferromagnetic, nonmagnetic, and ferromagnetic cases. The excitation spectrum is evaluated under rotation to investigate the local stability of the possible vortices and the vortex nucleation frequency.

PACS numbers: 03.75.Fi, 67.57.Fg

## I. INTRODUCTION

Much attention has been focused on Bose-Einstein condensation (BEC) realized in atomic gases [1, 2, 3, 4]. The atomic species investigated include the isotopes  $^{87}\text{Rb}$  and  $^{85}\text{Rb}$  and also  $^{23}\text{Na}$ ,  $^7\text{Li}$ , H,  $^4\text{He}$ , and  $^{41}\text{K}$  (see Refs. [1, 2, 3, 4, 5, 6, 7, 8]). These systems provide one with unique opportunities to investigate novel states of superfluid matter waves. When an atomic gas is cooled in an applied external magnetic field, the condensate is described by a scalar order parameter. The magneto-optic trapping method is widely used to study BEC. Recently it has become possible to trap an atomic gas using purely optical methods, thus the resulting BEC retains its original atomic hyperfine state. Specifically,  $^{23}\text{Na}$  [9] and  $^{87}\text{Rb}$  [10] both with  $F = 1$  are successfully Bose-condensed via optical trapping. This system, dubbed spinor BEC, is now described by multicomponent order parameter.

Ohmi and Machida [11], and Ho [12] have independently introduced the basic Hamiltonian for describing this spinor BEC by extending the Bogoliubov formalism to study the fundamental properties of this interesting multicomponent BEC, pointing out the richness of the topological defect configurations such as the  $l$ -vector textures and domain-wall structures. These are analogous to those found in the A and B phases of superfluid  $^3\text{He}$  [13, 14, 15]. An advantage of the dilute BEC systems with respect to strongly interacting liquid helium (for  $^4\text{He}$ , there exists no microscopic theory; for  $^3\text{He}$ , there is a BCS-like microscopic theory, generalized for  $p$ -wave pairing) is that for the dilute gas one can make controlled approximations, treating the interparticle interactions as small perturbative parameter. Moreover, it is possible to directly visualize the condensate in atomic gases using optical methods. Spin of condensate is easily controlled by external magnetic field. The BEC systems are quite versatile also in that the interaction parameter

can be adjusted over a large range — even its sign can be changed. Finally, the condensate in BEC systems can exhibit several spin states, *e.g.*, with the hyperfine spins  $F = 1$  and  $F = 2$ .

Theoretical studies of vortices and other topological defects in spinor BECs was initiated by Ohmi and Machida [11] and Ho [12]. Systematic investigations on vortices were followed by Yip [16] who considered both axisymmetric and non-axisymmetric vortices, and by Isoshima *et al.* [17], who only considered axisymmetric vortices and their excitation spectra. Leonhardt and Volovik [18], Stoof [19], Merzlin *et al.* [20], Zhou [21] and Martikainen and Suominen [22] examined exotic topological defect structures in spinor BECs.

Here we continue our studies of spinor BECs [11, 23, 24, 25, 26]; in particular, those on vortices with  $F = 1$  [17]. We investigate the vortex phase diagram in the plane spanned by the magnetization (which is given *a priori* when a three-component atomic gas is prepared) and the external rotation. We consider both the antiferromagnetic and ferromagnetic cases. The former is realized in  $^{23}\text{Na}$  while the latter is expected for  $^{87}\text{Rb}$ . The nonmagnetic situation in which the spin channel interaction  $g_s = 0$  is studied as the limiting case for  $|g_s| \ll g_n$  ( $g_s$  and  $g_n$  are the interaction constants for the spin and density channels). We restrict our calculations to axisymmetric vortices with winding numbers less than or equal to unity [17].

The organization of this paper is as follows: After giving a brief introduction to the Hamiltonian for the system and the extended Gross-Pitaevskii equation, we enumerate the possible vortices allowed by axisymmetry in Sec. 2. To investigate the global stability of the various vortex structures, the relative free energies of the different vortices are compared as functions of magnetization and rotation frequency in Sec. 3. Section 4 presents the excitation spectra for each vortex by solving the associated Bogoliubov equations extended to an order parameter with three components in order to investigate whether a given vortex state is stable against collective modes. This yields a local stability criterion for each vortex type. This consideration extends our previous works of nucleation criteria [27, 28, 29, 30, 31]. The final Section presents a

---

\*Electronic address: tomoya@focus.hut.fi

summary and discussion.

## II. POSSIBLE TYPES OF AXISYMMETRIC VORTICES

We treat the system of a Bose condensate with internal degrees of freedom  $F = 1$ . Hence the condensate order parameter is characterized by three components with  $m_F = 1, 0, -1$ . External rotation of the system around the rotation axis, perpendicular to the disc-shaped two-dimensional plane, is denoted by the angular velocity  $\Omega$  which has a sense (+ or -).

We start with the system Hamiltonian [11, 12]

$$\begin{aligned}
H = & \int d\mathbf{r} \left[ \sum_j \Psi_j^\dagger \{ -C\nabla^2 + V(\mathbf{r}) - \mu_j \} \Psi_j \right. \\
& + \frac{g_n}{2} \sum_{jk} \Psi_j^\dagger \Psi_k^\dagger \Psi_k \Psi_j \\
& + \frac{g_s}{2} \sum_\alpha \sum_{jklm} \Psi_j^\dagger \Psi_k^\dagger (F_\alpha)_{jl} (F_\alpha)_{km} \Psi_l \Psi_m \\
& \left. - \Omega \cdot \sum_j \Psi_j^\dagger (\mathbf{r} \times \mathbf{p}) \Psi_j \right] \quad (1)
\end{aligned}$$

with  $C = \hbar^2/(2m_a)$ . The interaction is characterized by the two kinds of channels; the density channel:  $g_n = 4\pi\hbar^2(a_0 + 2a_2)/(3m_a)$ , and the spin channel:  $g_s = 4\pi\hbar^2(a_2 - a_0)/(3m_a)$ . The atomic mass is  $m_a$ . The scattering lengths  $a_0$  and  $a_2$  characterize collisions between atoms with total spin 0 and 2. The subscripts are  $\alpha = (x, y, z)$  and  $i, j, k, l = (0, \pm 1)$ . The latter correspond to the above three species. The scalar field  $V(\mathbf{r})$  is the harmonic confining potential. The angular-momentum matrices  $F_\alpha$  are

$$\begin{aligned}
F_x &= \frac{1}{\sqrt{2}} \begin{pmatrix} 0 & 1 & 0 \\ 1 & 0 & 1 \\ 0 & 1 & 0 \end{pmatrix}, \\
F_y &= \frac{i}{\sqrt{2}} \begin{pmatrix} 0 & -1 & 0 \\ 1 & 0 & -1 \\ 0 & 1 & 0 \end{pmatrix}, \\
F_z &= \begin{pmatrix} 1 & 0 & 0 \\ 0 & 0 & 0 \\ 0 & 0 & 1 \end{pmatrix}.
\end{aligned} \quad (2)$$

The chemical potentials  $\mu_i$  obey  $\mu_1 - \mu_0 = \mu_0 - \mu_{-1}$ . We introduce  $\mu = \mu_0$  and  $\mu' = \mu_1 - \mu_0$ . The Gross-Pitaevskii equation for this system, extended to the three components becomes

$$\begin{aligned}
\sum_j \left[ \{ -C\nabla^2 + V(r) - (\mu + \mu' j) \} \delta_{jk} \right. \\
\left. + g_n \sum_l |\phi_l|^2 \delta_{jk} \right] \phi_k = 0. \quad (3)
\end{aligned}$$

The total energy of the condensate is given by

$$\begin{aligned}
E = & \int d^2\mathbf{r} \left[ \sum_j \phi_j^* (-C\nabla^2 + V(r)) \phi_j \right. \\
& + \frac{g_n}{2} \sum_{jk} |\phi_j|^2 |\phi_k|^2 + E_s \\
& \left. - i\hbar\Omega \cdot \sum_j \phi_j^* \nabla \phi_j \times \mathbf{r} \right], \quad (4)
\end{aligned}$$

where

$$E_s = \frac{g_s}{2} \sum_\alpha \left( \sum_{jk} \phi_j^* (F_\alpha)_{jk} \phi_k \right)^2. \quad (5)$$

Since we treat a cylindrically symmetric disc-shaped two-dimensional system, the condensate wavefunction  $\phi_j$  may be decomposed in the form:

$$\begin{aligned}
\phi_j(r, \theta) &= \phi_j(r) \gamma_j(\theta) \\
&= \phi_j(r) \exp[i(\alpha_j + \beta_j \theta)] \quad (6)
\end{aligned}$$

where the condensate wavefunctions  $\phi_j(\mathbf{r})$  ( $j = 0, \pm 1$ ) are expressed in terms of cylindrical coordinates. The phases of the condensate wavefunctions are determined such that the energy  $E_s$  in Eq. (5) is minimized. The minimizing of the above spin-dependent term:

$$\begin{aligned}
E_s(r) = & \frac{g_s}{2} \left[ 2\phi_0^2(r) \{ \phi_1^2(r) + \phi_{-1}^2(r) \right. \\
& + \phi_1(r)\phi_{-1}(r) (\gamma_1\gamma_{-1}\gamma_0^{*2} + \gamma_1^*\gamma_{-1}^*\gamma_0^2) \} \\
& \left. + (\phi_{-1}^2(r) - \phi_1^2(r))^2 \right] \quad (7)
\end{aligned}$$

leads to the condition

$$\gamma_1\gamma_{-1}\gamma_0^{*2} = \pm 1, \quad (8)$$

where the upper (lower) sign is used for the ferromagnetic (antiferromagnetic) case  $g_s < 0$  ( $g_s > 0$ ), respectively. This condition may be rewritten in terms of  $\alpha$  and  $\beta$  as

$$2\alpha_0 = \alpha_1 + \alpha_{-1} + n\pi \quad (9)$$

$$2\beta_0 = \beta_1 + \beta_{-1} \quad (10)$$

where  $n$  is an integer. We take  $\alpha_{\pm 1} = \alpha_0 = 0$  in the following since they have no effect in the discussion below. The phases of the three components are now expressed in the form

$$\begin{pmatrix} \gamma_1 \\ \gamma_0 \\ \gamma_{-1} \end{pmatrix} = \begin{pmatrix} \exp(i\beta\theta) \\ 1 \\ \pm \exp(-i\beta\theta) \end{pmatrix} \exp(i\beta_0\theta) \quad (11)$$

using  $\beta \equiv \beta_1 - \beta_0 = \beta_0 - \beta_{-1}$ . In Fig. 1, the various lines show the possible combinations of the  $\beta_i$ , giving rise to the vortex types which we consider in the following. If we restrict our consideration to the phase coefficient, or the winding number being less than 2, there are nine possible combinations of the  $\beta_i$ . There is one vortexfree configuration and the other combinations are (1,0,-1), (1,1,1), and  $(1, \frac{1}{2}, 0)$  where the winding numbers of the three components  $\phi_1$ ,  $\phi_0$ , and  $\phi_{-1}$  are denoted in this order. The latter vortex configuration is only realized in a form  $(1,x,0)$  where  $\phi_0$  vanishes (where  $\beta_i$  is fractional). It should be noted that the restriction for the winding number to be less than 2 is reasonable, because a vortex with a higher winding number is unstable and easily breaks up into vortices with unit winding number.

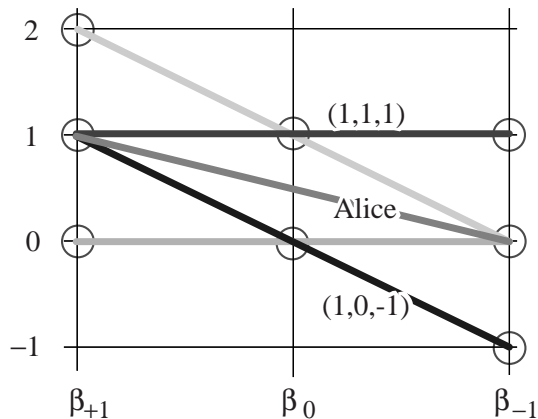


FIG. 1: Possible allowed vortex configurations under axisymmetry. Each condensate  $\phi_i$  ( $i = 1, 0, -1$ ) has the phase  $\beta_i$ . The vortices; (1,0,-1), (1,x,0) and (1,1,1) are treated in this paper.

### III. RELATIVE STABILITY OF VARIOUS VORTICES

We compare the relative energies of the various vortices enlisted above. There are eight candidates for the possible vortex type, allowed by axisymmetry. Three of them are (1,0,-1), (1,1,1), and  $(1,x,0)$  where “x” denotes that this component vanishes identically as mentioned above. The last one is named Alice vortex after the Alice string [18]. By interchanging the roles of  $\phi_1$  and  $\phi_{-1}$ , we can obtain two more vortices:  $(-1,0,1)$ , and  $(0,x,1)$ . The remaining combinations  $(0,x,1)$ ,  $(-1,x,0)$  and  $(-1,-1,-1)$  always have higher energies than those of  $(0,x,1)$ ,  $(1,x,0)$  and  $(1,1,1)$ , respectively, when the external angular velocity  $\Omega$  is positive. Thus, in what follows, we consider the vortices, (1,0,-1), (1,1,1),  $(1,x,0)$ ,  $(-1,0,1)$ , and  $(0,x,1)$  for  $\Omega \geq 0$  and  $M/N \geq 0$ .

The mass of a  $^{87}\text{Rb}$  atom is  $m_a = 1.443 \times 10^{-25}\text{kg}$ . This value is used in the following. We use the scattering lengths  $a_0 = 5.5 \times 10^{-9}\text{m}$  and  $a_2 = 5.843 \times 10^{-9}\text{m}$

for the antiferromagnetic case. The ratio of the interaction coefficients is  $g_s/g_n = +0.02$ . Another set for the ferromagnetic case is  $a_0 = 5.5 \times 10^{-9}\text{m}$  and  $a_2 = 5.182 \times 10^{-9}\text{m}$ , whose ratio of the interaction coefficients is  $g_s/g_n = -0.02$ . The coefficient of the magnetic term vanishes when  $a_0 = a_2 = 5.5 \times 10^{-9}\text{m}$ . The ratio becomes  $g_s/g_n = 0$ . The amplitude of the ratio  $|g_s/g_n| = 0.02$  is for a Na atom.

For each vortex type and the  $g_s$  and  $\mu'$ , the chemical potential  $\mu$  is determined such that the linear density of the particle number becomes  $2 \times 10^3(\mu\text{m})^{-1}$ . We use a harmonic potential with  $\nu = 200\text{Hz}$  for radial confinement. All the energies are scaled by the trap frequency  $\hbar\nu$ . The angular velocity  $\Omega$  is normalized by  $2\pi\nu$  below.

The spatial profile of the condensate wavefunctions in each vortex is determined by the above GP Eq. (3), which is expressed as

$$\sum_k \left[ \{-C\nabla^2 + V(r) - (\hbar\Omega\beta_0 + \mu) - j(\hbar\Omega\beta + \mu') + g_n \sum_l |\phi_l|^2 n\} \delta_{jk} + g_s \sum_\alpha (F_\alpha)_{jk} \sum_{lm} (F_\alpha)_{lm} \phi_l^* \phi_m \right] \phi_k = 0. \quad (12)$$

When we vary  $\Omega$  and  $\mu'$ , the condensate wavefunctions  $\phi_i$  are determined by a single parameter  $\hbar\Omega\beta + \mu'$  because the variation of  $\hbar\Omega\beta_0$  is canceled by that of the chemical potential  $\mu$ .

The energy of the system Eq. (4) is rewritten as

$$\begin{aligned} E &= \int d^2\mathbf{r} \left[ \sum_j \phi_j^* (-C\nabla^2 + V(r)) \phi_j + \frac{g_n}{2} \sum_{jk} |\phi_j|^2 |\phi_k|^2 + E_s(r) \right] - \sum_j \hbar\Omega(\beta_0 + j\beta) N_j \\ &= E_{\text{inner}} - \hbar\Omega L, \end{aligned} \quad (13)$$

where the number of particles in the  $j$ 'th component is  $N_j = \int d^2\mathbf{r} |\phi_j|^2$ . The total particle number in the system is  $N = \sum_j N_j$ , and the total angular momentum is  $L = \sum_j (\beta_0 + j\beta) N_j$ . The energy  $E_{\text{inner}}$ , the magnetization  $M = \sum_j j N_j$ , and  $L$  are functions of the  $\phi_j$  and, therefore, are functions of  $\hbar\Omega\beta + \mu'$ . The critical angular velocity  $\Omega_c$  for a given magnetization between two vortex types (1) and (2) is simply determined by

$$\hbar\Omega_c(M) = \frac{E_{\text{inner}}^{(1)} - E_{\text{inner}}^{(2)}}{L^{(1)} - L^{(2)}}. \quad (14)$$

The range of  $M$  which a vortex state can take depends on the interaction constant  $g_s$  and the winding number. For example, the (1,1,1) vortex does not have an intermediate value of  $M/N$  in the cases with  $g_s = 0$  (non-magnetic case) and  $-0.02g_n$  (ferromagnetic case). This behavior is well known for the uniform spinor condensate [11, 12]. When  $g_s = -0.02g_n$ , the magnetization

range  $-1 < M/N < 0$  is not allowed for the  $(1,x,0)$  vortex. This range may be improved with improved numerical accuracy [29, 32].

Figure 2 shows the phase diagrams with the lowest energy in the plane of  $M/N$  and  $\Omega$  for the three cases; the antiferromagnetic ( $g_s = 0.02g_n$ ), the nonmagnetic ( $g_s = 0$ ), and the ferromagnetic cases ( $g_s = -0.02g_n$ ). The critical angular velocity  $\Omega_c(M)$  in Eq. (14) determines the boundaries of each domain. When the system is antiferromagnetic or nonmagnetic, the  $(0,x,1)$  vortex has the lowest energy around  $\Omega = 0$  for  $M/N = 1$ . This is because the  $(0,x,1)$  vortex almost reduces to the vortexfree single-component state without the vortex winding in the full polarization limit.

The  $(1,0,-1)$  vortex is lowest in energy around  $\Omega = 0$  with  $M/N = 0$ , irrespective of the magnetism. The condensate simply becomes a vortexfree system for the ferromagnetic case. For the antiferromagnetic case, the nonrotating  $\phi_0$  component without winding number dominates and the  $\phi_1$  and  $\phi_{-1}$  components which have opposite winding numbers are small.

This  $(1,0,-1)$  vortex and the Alice vortex compete in the region around  $\Omega \sim 0.6, M/N \sim 0.8$ . The curve between them reflects the kinetic energy of the  $(1,0,-1)$  vortex when there is no magnetic term ( $g_s = 0$ ). The amplitudes of the condensate wavefunctions  $\phi_1(r)$  and  $\phi_0(r)$  of the  $(1,0,-1)$  vortex for the magnetization  $M/N(> 0)$  are equal to  $\phi_1(r)$  and  $\phi_{-1}(r)$  of the  $(1,x,0)$  vortex for the magnetization  $2M/N - 1$ . The  $(1,0,-1)$  and the  $(1,x,0)$  vortex have the angular momenta  $L = M$  and  $L = (M + N)/2$ , respectively. The critical  $\Omega_c$  in Eq. (14) becomes

$$\hbar\Omega_c(M) = 2 \frac{E'_{\text{inner}}(M) - E'_{\text{inner}}((M + N)/2)}{M - N} \quad (15)$$

where  $E'_{\text{inner}}(M)$  is  $E_{\text{inner}}$  of the  $(1,0,-1)$  vortex for  $0 < M < N$ . The behavior of  $\Omega_c$  is still complicated because both the numerator and the denominator approach zero when  $M$  approaches  $N$ .

#### IV. LOCAL STABILITY

There is another stability criterion for a vortex. The excitation spectrum for a stable vortex must be positive definite. In other words, if the lowest excited state in the spectrum becomes negative as a function of  $\Omega$ , the given vortex becomes locally unstable.

##### A. Excitation spectrum

The excitation spectrum is obtained by solving the following Bogoliubov equation extended to the three-component BEC case:

$$\sum_k \{A_{jk}u_q(\mathbf{r}, k) - B_{jk}v_q(\mathbf{r}, k)\} = \varepsilon_q u_q(\mathbf{r}, j),$$

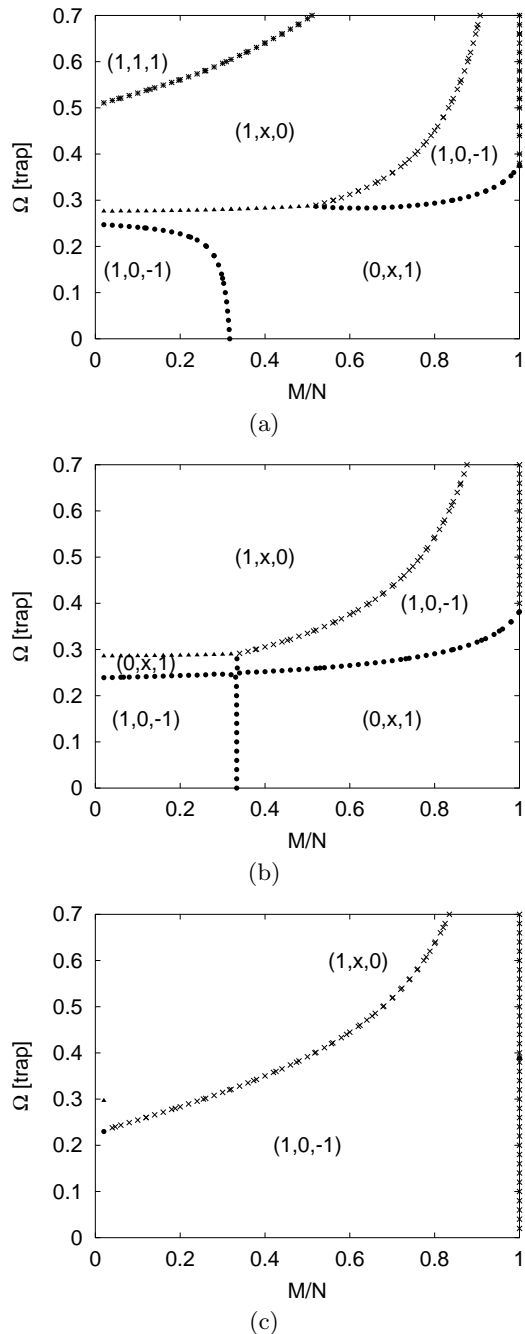


FIG. 2: Phase diagrams in the  $\Omega$  vs  $M/N$  plane, showing the vortex type which has the lowest energy  $E(\Omega)$ . (a) Antiferromagnetic case ( $g_s = 0.02g_n$ ). (b) Nonmagnetic case ( $g_s = 0$ ). (c) Ferromagnetic case ( $g_s = -0.02g_n$ ). The  $(1,1,1)$  vortex is absent from the phase diagrams (b) and (c) because this vortex cannot have a stable configuration for  $-1 < M/N < 1$ . The  $(0,x,1)$  Alice vortex is not stabilized and it is thus excluded from the phase diagram (c).

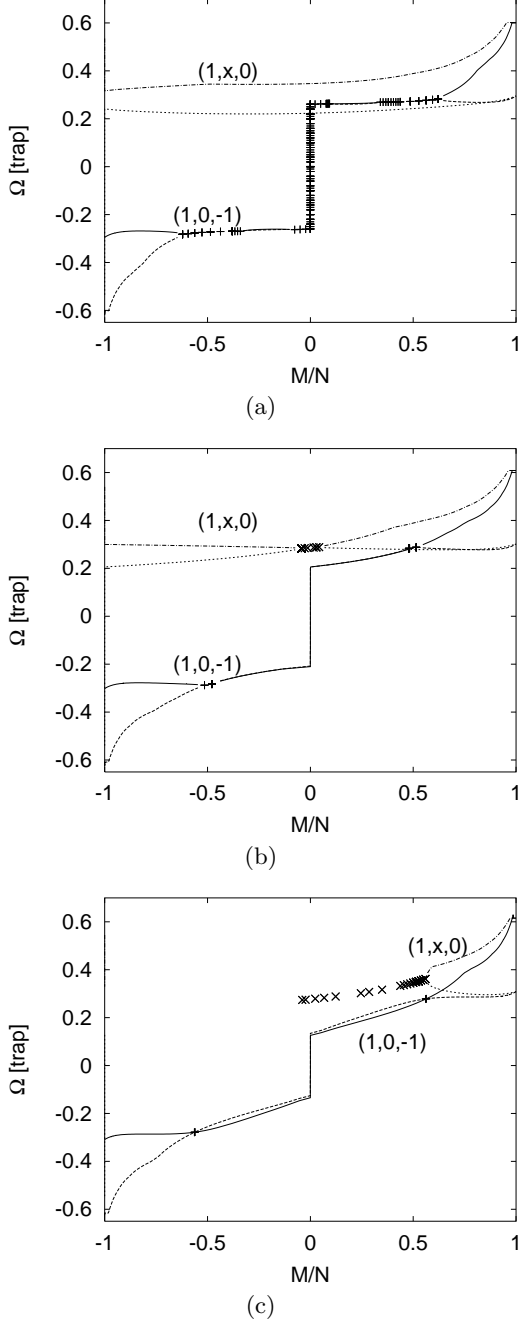


FIG. 3: Local stability regions bounded by  $\Omega_c^\pm$  for the two types of vortices, (1,0,-1) and (1,x,0). (a) Antiferromagnetic case ( $g_s = 0.02g_n$ ). (b) Nonmagnetic case ( $g_s = 0$ ). (c) Ferromagnetic case ( $g_s = -0.02g_n$ ). The solid line and the dashed line show the upper critical  $\Omega_c^+$  and the lower critical  $\Omega_c^-$  for a (1,0,-1) vortex. The dashed-dotted line and the dotted line show the upper critical  $\Omega_c^+$  and the lower critical  $\Omega_c^-$  for the (1,x,0) Alice vortex. The lower critical  $\Omega$  is higher than the upper critical  $\Omega$  for  $-0.5 < M/N < 0.5$  in the (1,0,-1) vortex. The range  $-1 < M/N < -0.1$  for the (1,x,0) vortex is inhibited because of the ferromagnetic interaction. When the imaginary part of  $\varepsilon$  is finite, its real part is used in Eqs. (24) and (25). These regions are indicated with the crosses and pluses.

$$\sum_k \{B_{jk}^* u_q(\mathbf{r}, k) - A_{jk}^* v_q(\mathbf{r}, k)\} = \varepsilon_q v_q(\mathbf{r}, j) \quad (16)$$

where

$$\begin{aligned} A_{jk} = & \{-C\nabla^2 + V(r) - (\mu + j\mu')\}\delta_{jk} \\ & + g_n \left\{ \sum_l |\phi_l|^2 \delta_{jk} + \phi_j \phi_k^* \right\} \\ & + g_s \sum_\alpha \sum_{lm} \left[ (F_\alpha)_{jk} (F_\alpha)_{lm} \phi_l^* \phi_m \right. \\ & \left. + (F_\alpha)_{jm} (F_\alpha)_{lk} (\phi_l^* \phi_m) \right] \\ & - i\hbar\Omega \cdot \nabla \times \mathbf{r} \delta_{jk}, \end{aligned} \quad (17)$$

$$B_{jk} = g_n \phi_j \phi_k + g_s \sum_\alpha \sum_{lm} (F_\alpha)_{jl} \phi_l (F_\alpha)_{km} \phi_m. \quad (18)$$

where  $u_q(\mathbf{r}, i)$  and  $v_q(\mathbf{r}, i)$  are the  $q$ 'th eigenfunctions with the spin component  $i$  and  $\varepsilon_q$  corresponds to the  $q$ 'th eigenvalue. The normalization condition for the  $u_q(\mathbf{r}, i)$  and  $v_q(\mathbf{r}, i)$  is

$$\sum_i \int \{|u_q(\mathbf{r}, i)|^2 - |v_q(\mathbf{r}, i)|^2\} d\mathbf{r} = 1. \quad (19)$$

In our disc-shaped system, the wavefunctions have the phase  $u_q(\mathbf{r}, j) = u_q(r, j)e^{i\theta(q\theta + \beta_0 + j\beta)}$  and  $v_q(\mathbf{r}, j) = v_q(r, j)e^{i\theta(q\theta - \beta_0 - j\beta)}$ . Then Eqs. (16 - 18) are written as

$$\begin{aligned} & \sum_j \{X_{ij}^+ u_q(r, j) - 2Z_{ij} v_q(r, j)\} \\ & = (\varepsilon_q + \hbar\Omega q\theta) u_q(r, i) \end{aligned} \quad (20)$$

$$\begin{aligned} & \sum_j \{2Z_{ij}^* u_q(r, j) - X_{ij}^- v_q(r, j)\} \\ & = (\varepsilon_q + \hbar\Omega q\theta) v_q(r, i) \end{aligned} \quad (21)$$

where

$$\begin{aligned} X_{ij}^\pm = & [-C \left\{ \frac{d^2}{dr^2} + \frac{1}{r} \frac{d}{dr} + \frac{(q\theta \pm (\beta_0 + \beta j))^2}{r^2} \right\} \\ & + V(r) - (\mu + j\mu') + g_n \sum_k |\phi_k|^2 \delta_{ij} \\ & + g_n (\phi_j^* \phi_i) \pm \hbar\Omega(\beta_0 + \beta j) \delta_{ij} \end{aligned} \quad (22)$$

$$Z_{ij} = g_n \phi_i \phi_j + g_s \sum_\alpha \sum_{kl} \phi_k \phi_l (F_\alpha)_{il} (F_\alpha)_{jk}. \quad (23)$$

The excitation energy  $\varepsilon_q$  varies as a function of the angular velocity  $\Omega$  as determined by Eqs. (16) and (21). The critical values for local stability are defined by

$$\Omega_c^+ = \min_{q\theta > 0} (\varepsilon_q / q\theta) \quad (24)$$

$$\Omega_c^- = \max_{q\theta < 0} (\varepsilon_q / q\theta). \quad (25)$$

The critical velocity  $\Omega_c^+$  defined above corresponds to the instability of the surface excitations; namely, the energy of the excitation modes for  $q\theta > 0$  become negative

(see the paper [28] by Isoshima and Machida for the one-component BEC). The critical velocity  $\Omega_c^-$  corresponds to the local instability where the core excitation modes with  $q_\theta < 0$  become negative upon varying  $\Omega$ . In the following, we determine  $\Omega_c^\pm$ , yielding a stability region in the  $\Omega$  vs  $M/N$  plane where the all excitation modes are positive definite for a given vortex configuration. Namely, we evaluate  $\Omega_c^\pm$  for the vortex types (1,0,-1), (1,1,1), and (1,x,0) as functions of  $\Omega$  and  $M/N$ .

When there is a mode with  $q_\theta = 0$  and  $\varepsilon < 0$ , the system has an instability regardless of external rotation and the definition of  $\Omega_c^\pm$  becomes meaningless. There are few modes found with  $\varepsilon < 0$  for  $q_\theta = 0$ . The value is at  $-10^{-12} < \varepsilon < 0$ . There is also a complex mode with  $q_\theta = 0$ . The real part is small ( $\text{Re}(\varepsilon) < 10 \times 10^{-13}$ ) while the imaginary part is of order  $O(0.01)$ . We ignore them as the modes degenerate with the condensate.

## B. Local stability region

Let us investigate  $\Omega_c^\pm$  for the (1,0,-1), (1,x,0), and (1,1,1) vortices. Figures 3(a), 3(b), and 3(c) show the local stability regions for each vortex where all the excitation modes have positive eigenvalues. Figure 4 shows the radial shape and  $q_\theta$  of the wavefunctions which correspond to the critical value  $\Omega_c^\pm$ .

### 1. Similarity to scalar system

The  $\Omega_c^\pm$  of the (1,0,-1) vortex for  $M/N = \pm 1$  and of the Alice vortex for  $M/N = 1$  may be understood as those of a vortex in a scalar BEC. The  $\Omega_c^\pm$  in Fig. 3 reduces to those of the one-component vortex system for  $M/N = 1$  because the fully polarized case is nothing but a one-component BEC with a single vortex. When we decrease  $M/N$  towards  $-1$ , the (1,0,-1) vortex becomes a single-component system again with the opposite winding number and the critical  $\Omega_c^\pm$ 's have opposite signs.

As seen in Fig. 4, the modes responsible for  $\Omega_c^+$  are localized on the edge of the condensate ( $r \simeq 3\mu\text{m}$ ) and have a large angular momentum  $q_\theta \simeq 7$  when  $M/N > 0.9$  in both the (1,0,-1) and (1,x,0) vortices. This implies a surface-instability mode similar to the surface mode in a scalar vortex. The mode remains at the edge of the condensate for  $M/N > 0.8$ .

The angular momenta of the modes of  $\Omega_c^-$  are  $-1$  over most of the regions: for  $0 < M/N \leq 1$  in the (1,0,-1) vortex and for  $-1 < M/N \leq 1$  in the Alice vortex. This mode is localized at the center when the condensate has a large angular momentum [ $M/N = 1$  in Figs. 4(a), 4(b), 4(c)]. This feature arises from the localized core state in a scalar vortex.

### 2. Characteristic of spinor system

The spatial extent of the modes of  $\Omega_c^-$ , which are localized around the core for large  $M/N$  expands as  $M/N$  decreases. This is shown for  $M/N = 0$  in Figs. 4(a) and 4(b), and for  $M/N = -1$  in Figs. 4(c). This is common to both the (1,0,-1) and (1,x,0) vortices. The wavefunction has a shape similar to that of the condensate and a spin structure different from the condensate. Thus this instability at  $\Omega_c^-$  means a spin-flip instability. This is also true for  $\Omega_c^+$  of the (1,0,-1) vortex for  $-0.5 < M/N < 0.5$ . The shape of the wavefunctions is similar to that of the condensate. This is not the situation in the antiferromagnetic case. The wavefunction of  $\Omega_c^+$  indicates a single vortex of the -1 component rather than the non-vortex -1 component, as shown in Fig. 4 (b).

According to Figs. 3 (a-c), the critical values  $\Omega_c^+$  and  $\Omega_c^-$  of the (1,0,-1) vortex are close to each other for  $-0.5 < M/N < 0.5$ . There is no range of  $\Omega$  to stabilize the system in the ferromagnetic case because  $\Omega_c^- > \Omega_c^+$ . This range is quite narrow in the antiferromagnetic case (*e.g.*,  $0.261 < |\Omega| < 0.263$  for  $M/N = \pm 0.2$ ).

The (1,x,0) vortex reduces to the vortexfree system near  $M/N = -1$ . As shown in Figs. 3(a) and 3(b), there is an instability for  $\Omega = 0$  unlike the vortexfree scalar system. Figure 4(c) shows the shape of the wavefunctions  $u$  and  $v$  of  $\Omega_c^-$ . The shape resembles that of the condensate. This instability indicates that the whole condensate may have the +1 component without winding number. The winding-number combination of the (1,x,0) vortex turns into (0,0,0). When  $\mu'$  is large and negative,  $\Omega_c^+$  and  $\Omega_c^-$  become about 0.5 and  $-0.3$  respectively. Therefore, the system is stable for  $\Omega = 0$  just like the vortexfree scalar system. The  $\Omega_c^\pm$  shift, depending on  $\mu'$ , even when  $M/N$  has the fixed value  $-1$ . This is because our calculation does not include the magnetization from the non-condensate.

### 3. Complex eigenvalues

Complex eigenvalues emerge when two levels with the opposite angular momenta and the same eigenvalues happen to appear. The complex eigenvalues of Bogoliubov equations have been reported for multiply quantized vortex of scalar BEC [33] and vortex states of binary BEC [34]. When the eigenvalue  $\varepsilon_q$  has a complex value, the left-hand side of Eq. (19) becomes zero. We still adopt the real part of such eigenvalues because continuity of the real eigenvalues and the real part of complex eigenvalues as shown in Fig. 3 seems physically meaningful.

### 4. The (1,1,1) vortex

As for the (1,1,1) vortex, neither the ferromagnetic nor the nonmagnetic states can assume intermediate values

of magnetization and  $M/N$  becomes  $\pm 1$ . Even at each magnetization,  $\Omega_c^\pm$  varies with the chemical potential  $\mu'$ . The maximum value of  $\Omega_c^-$  is about 1.8 (in trap units). The wavefunction corresponding to  $\Omega_c^-$  is localized at the center and has a spin component different from that of the condensate. The minimum value of  $\Omega_c^+$  is about 0.4. Because  $\Omega_c^-$  is always larger, the (1,1,1) vortex is always unstable in the sense of local stability.

This is also the case for the antiferromagnetic system.  $\Omega_c^- \simeq 1.8$  and  $\Omega_c^+ \simeq 0.4$  mean that the (1,1,1) vortex is locally unstable. When the chemical potential  $\mu'$  is large enough, these critical values  $\Omega_c^\pm$  reduce to  $\Omega_c^+ = 0.6$  and  $\Omega_c^- = 0.3$ .

## V. DISCUSSION

We have determined the vortex phase diagram in the plane of external rotation frequency  $\Omega$  vs relative magnetization  $M/N$  of a spinor BEC system for the cases of antiferromagnetic ( $g_s > 0$ ), nonmagnetic ( $g_s = 0$ ), and ferromagnetic ( $g_s < 0$ ) interactions. By solving the extended Gross-Pitaevskii equation for the spinor  $F=1$  BEC with the three components ( $m_F = 1, 0, -1$ ), we have investigated the relative stability of the possible axisymmetric vortices which are classified according to their winding numbers for each component; namely, (1,0,-1), (1, $x$ ,0), and (1,1,1) for  $(\phi_1, \phi_0, \phi_{-1})$ . The excitation spectra are also studied to find the stability regions for each vortex in the  $\Omega$  and  $M/N$  plane. This allows us to estimate the vortex nucleation frequency in the actual experiment (for details, see Refs. [28, 31] for the correspondence between local stability and nucleation frequency).

Yip [16] has studied the two non-axisymmetric vortices in addition to the present axisymmetric vortices within the GP equation under a particular rotation frequency ( $\Omega \sim 0.4$  in our notation) for the antiferromagnetic case only. This corresponds to Fig. 2(a) for  $\Omega \sim 0.4$ . Although the lower  $M/N$  region ( $0 < M/N < 0.2$ ) is occupied by a non-axisymmetric vortex, in the remaining region the (1, $x$ ,0) vortex is stabilized over the non-axisymmetric vortex, coinciding with our result. We believe that the present phase diagram remains valid over a broad region even taking into account non-axisymmetric vortices. This is because a large part of Yip's phase diagram is covered by axisymmetric vortices (see Fig.1 in Yip's paper [16]). In the future we aim to take into account the non-axisymmetric vortex in addition to the present axisymmetric ones. This kind of a calculation must be performed with the help of the excitation spectrum, which signals the instability towards a more stable vortex configuration, for each vortex and is needed to predict the experimentally realized vortices in a spinor BEC.

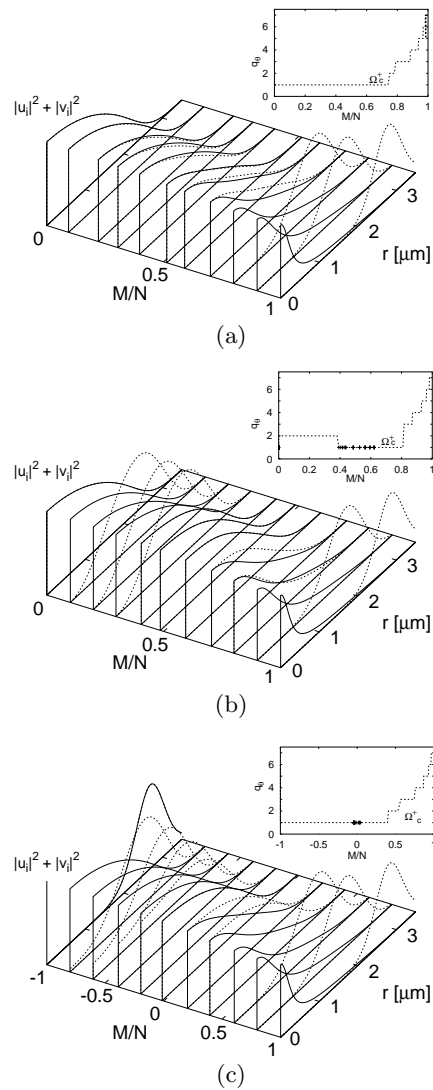


FIG. 4: Spatial variations of  $\sum_i (|u_q(r, i)|^2 + |v_q(r, i)|^2)$  as a function of the radial direction corresponding to the collective mode at  $\Omega_c^\pm$  for each  $M/N$  is plotted. The (dotted) lines corresponds to  $\Omega_c^-$  ( $\Omega_c^+$ ) When the eigenfunctions  $u_i$  and  $v_i$  are complex number, the sum of the real part  $\sum_i (\text{Re}(u_q(r, i))^2 + \text{Re}(v_q(r, i))^2)$  is plotted instead. Inset of each figure shows the angular momentum index  $q_\theta$  of the mode corresponding to  $\Omega_c^\pm$ . When  $M/N = 1$ , the mode of  $\Omega_c^+$  has a peak at the edge of the condensate ( $r \sim 2\mu\text{m}$ ) and the mode at  $\Omega_c^-$  has a peak at the vortex center ( $r = 0$ ). These reproduce the result of the scalar BEC. When  $M/N = 1$ ,  $q_\theta = 7$  and it reduces to 1 as  $M/N$  decreases. (a) (1,0,-1) vortex in the ferromagnetic case. (b) (1,0,-1) vortex in the antiferromagnetic case. (c) (1, $x$ ,0) vortex in the nonmagnetic case.

### Acknowledgements

The authors thank T. Ohmi, T. Mizushima, T. Kita, M. M. Salomaa, S. M. M. Virtanen, and T. Simula for

useful discussions.

- 
- [1] M. H. Anderson, J. R. Ensher, M. R. Matthews, C. E. Wieman and E. Cornell, *Science* **269**, 198 (1995).
- [2] C. C. Bradley, C. A. Sackett, J. J. Tollett and R. G. Hulet, *Phys. Rev. Lett.* **75**, 1687 (1995).
- [3] K. B. Davis, M.-O. Mewes, M. R. Andrews, N. J. van Druten, D. S. Durfee, D. M. Kurn and W. Ketterle, *Phys. Rev. Lett.* **75**, 3969 (1995).
- [4] C. J. Pethick and H. Smith, *Bose-Einstein Condensation in Dilute Gases* (Cambridge University Press, 2002).
- [5] S. L. Cornish, N. R. Claussen, J. L. Roberts, E. A. Cornell and C. E. Wieman, *Phys. Rev. Lett.* **85**, 1795 (2000).
- [6] D. G. Fried, T. C. Killian, L. Willmann, D. Landhuis, S. C. Moss, D. Kleppner and T. J. Greytak, *Phys. Rev. Lett.* **81**, 3811(1998).
- [7] A. Robert, O. Sirjean, A. Browaeys, J. Poupard, S. Nowak, D. Boiron, C. I. Westbrook and A. Aspect, *Science* **292**, 461 (2001).
- [8] G. Modugno, G. Ferrari, G. Roati, R.J. Breecha, A. Simoni and M. Inguscio, *Science* **294**, 1320 (2001).
- [9] J. Stenger, S. Inouye, D. M. Stamper-Kurn, H.-J. Miesner, A. P. Chikkatur and W. Ketterle, *Nature* **369**, 345 (1998). H.-J. Miesner, D. M. Stamper-Kurn, J. Stenger, S. Inouye, A. P. Chikkatur and W. Ketterle, *Phys. Rev. Lett.* **82**, 2228(1999). D. M. Stamper-Kurn, H.-J. Miesner, A. P. Chikkatur, S. Inouye, J. Stenger and W. Ketterle, *Phys. Rev. Lett.* **83**, 661 (1999).
- [10] M. Barrett, J. Sauer and M.S. Chapman, *Phys. Rev. Lett.* **87**, 010404 (2001).
- [11] T. Ohmi and K. Machida, *J. Phys. Soc. Jpn.* **67** (1998) 1822.
- [12] T.-L. Ho, *Phys. Rev. Lett.* **81**, 742. (1998).
- [13] M. M. Salomaa and G. E. Volovik, *Rev. Mod. Phys.* **59**, 533 (1987).
- [14] M. M. Salomaa and G. E. Volovik, *Phys. Rev. B.* **37**, 9298 (1988).
- [15] M. M. Salomaa and G. E. Volovik, *J. Low Temp. Phys.* **74**, 319 (1989).
- [16] S.-K. Yip, *Phys. Rev. Lett.* **83**, 4677 (1999).
- [17] T. Isoshima, K. Machida and T. Ohmi, *J. Phys. Soc. Jpn.* **70**, 1604 (2001).
- [18] U. Leonhardt and G. E. Volovik, *JETP Lett.* **72**, 46 (2000).
- [19] H.T.C. Stoof, cond-mat/0002375.
- [20] Karl-Peter Marzlin, Weiping Zhang and Barry C. Sanders, *Phys. Rev. A* **62**, 13602 (2000).
- [21] Fei Zhou, *Phys. Rev. Lett.* **87**, 080401 (2001).
- [22] J.-P. Martikainen and K.-A. Suominen, cond-mat/0106013.
- [23] T. Isoshima, K. Machida and T. Ohmi, *Phys. Rev. A* **60**, 4857 (1999).
- [24] T. Isoshima, M. Nakahara, T. Ohmi and K. Machida, *Phys. Rev. A* **61**, 063610 (2000).
- [25] M. Nakahara, T. Isoshima, K. Machida, S. Ogawa and T. Ohmi, *Physica B* **284-288**, 17 (2000).
- [26] T. Isoshima, T. Ohmi and K. Machida, *J. Phys. Soc. Jpn.* **69**, 3864 (2000).
- [27] T. Isoshima and K. Machida, *J. Phys. Soc. Jpn.* **66**, 3502 (1997).
- [28] T. Isoshima and K. Machida, *J. Phys. Soc. Jpn.* **68**, 487 (1999).
- [29] T. Isoshima and K. Machida, *Phys. Rev. A* **59**, 2203 (1999).
- [30] T. Isoshima and K. Machida, *Phys. Rev. A* **60**, 3313 (1999).
- [31] T. Mizushima, T. Isoshima and K. Machida, *Phys. Rev. A* **64**, 043610 (2001).
- [32] S. M. M. Virtanen, T. P. Simula and M. M. Salomaa, *Phys. Rev. Lett.* **86**, 2704 (2001).
- [33] H. Pu, C. K. Law, J. H. Eberly, and N. P. Bigelow, *Phys. Rev. A* **59**, 1533 (1999).
- [34] D. V. Skryabin, *Phys. Rev. A* **63**, 013602 (2000).